1 Theoretical Derivation of Aerosol Lidar Ratio using Mie
2 Theory for CALIOP-CALIPSO and OPAC Aerosol Models

3 Radhika A. Chipade[1] and Mehul R. Pandya[1]

4 [1]Space Applications Centre (ISRO), Ahmedabad, Gujarat, India – 380015.

5 *Correspondence to*: Radhika A. Chipade (radhikachipade@gmail.com)

6 **Abstract.** The extinction-to-backscattering ratio, popularly known as lidar (light detection and ranging) ratio of

7 atmospheric aerosols is an important optical property, which is essential to retrieve the extinction profiles of

8 atmospheric aerosols. Lidar satellite observations can provide the global coverage of atmospheric aerosols along

9 with their vertical extent. NASA's Cloud-Aerosol Lidar with Orthogonal Polarisation (CALIOP) on-board Cloud-

10 Aerosol Lidar and Infrared Pathfinder Satellite Observations (CALIPSO) is the only space-based platform

11 available so far, that provides the vertical profiles of extinction due to atmospheric aerosols. A physics-based

12 theoretical approach is presented in the present paper that estimates lidar ratio values for CALIPSO aerosol

13 models, which can be used as inputs to determine the extinction profiles of aerosols using CALIPSO data. The

14 developed methodology was also qualified by comparing it with the lidar ratio values derived using AERONET

15 datasets. Lidar ratio for CALIPSO aerosols models were estimated in the range of 38.72 sr to 85.98 sr at 532 nm

16 whereas, at 1064 nm lidar ratio varied between 20.11 sr to 71.11 sr depending upon the aerosol type and their size

17 distributions.

18 Aerosols are compositions of various particles and thus the presence of water vapour in the atmosphere can affect

19 the optical properties of the aerosols. Thus, the effect of relative humidity on lidar ratio was studied using Optical

20 Properties of Cloud and Aerosols software tool (OPAC) aerosol models, which are the standard aerosol models

21 against the cluster classified AERONET and CALIPSO aerosol models. Water soluble particles contribute

22 substantially in clean continental, clean marine, tropical marine and desert aerosol models and are hygroscopic in

23 nature. Hygroscopic sulfate particles dominate the Antarctic aerosols during summertime. In presence of relative

24 humidity between 0 – 80%, the lidar ratio values were observed to decrease from 53.59 sr to 47.13 sr, 53.66 sr to

25 47.15 sr, 53.70 sr to 47.16 sr and 55.32 sr to 48.78 sr at 532 nm for clean continental, clean marine, tropical marine

26 and desert aerosols respectively, whereas lidar ratio gradually increased from 47.13 sr to 51 sr, 47.15 sr to 51 sr,

27 47.16 sr to 51 sr and 48.78 sr to 51.68 sr respectively for these aerosol models when relative humidity was between

28 80 – 99%; due to constituent hygroscopic particles. In case of Antarctic aerosols, the lidar ratio was observed to

29 increase from 57.73 sr to 97.64 sr due to hygroscopic sulfate particles that backscattered heavily in presence of

30 water vapour at 532 nm. The soot particles dominate the polluted continental and polluted marine particles causing

31 an increase in lidar ratio over corresponding clean counterpart. Similar results were observed at 1064 nm for

32 OPAC aerosol models.

33 1 Introduction:

34 The light detection and ranging (lidar) measurements are considered appropriate to retrieve the range-resolved

35 values of vertical backscatter and extinction profiles of tropospheric aerosols. The single scattering lidar equation

36 is solved in order to determine extinction and backscatter profiles of aerosols, which depends on the ratio of

37 extinction-to-backscatter coefficient, known as lidar ratio. Thus, estimation of lidar ratio is essential to solve the

38 lidar equation and important in the study of climatic impact of aerosols.

39 Many researchers have reported the lidar ratio estimation as a part of retrieval of extinction and backscatter profiles

40 of tropospheric aerosols using ground as well as satellite data. Takamura et al. (1994) derived lidar ratio combining

41 the measurements from lidar, sunphotometer and optical particle counter. Lidar ratio can be directly estimated

42 using the Raman lidar. Ansmann et al. (2002) demonstrated that the lidar ratio retrieved using Raman lidar can be

43 used to retrieve extinction profiles of the aerosols using elastic backscatter lidar. The National Aeronautics And

44 Space Administration's (NASA's) Cloud-Aerosol Lidar with Orthogonal Polarisation (CALIOP) on-board Cloud-

45 Aerosol Lidar and Infrared Pathfinder Satellite Observations (CALIPSO) launched in 2006 is the only available

46 source of satellite data to retrieve vertical profiles of tropospheric aerosols. CALIOP is an elastic backscatter lidar

47 (Hunt et al. 2009) that records the backscatter photon counts due to tropospheric aerosols and the vertical

48 extinction and backscatter profiles of aerosols are retrieved solving the single scattering lidar equation (Young

49 and Vaughan 2009). This retrieval process uses a look-up table approach for lidar ratio in order to solve the lidar

50 equation. The lidar ratio selection scheme used for CALIOP-CALIPSO products is based on cluster analysis of

51 aerosol measurements using data recorded at several AERONET network stations spread across the globe (Omar

52 et al. 2009, Young and Vaughan 2009). Thus, a novel theoretical approach is presented in the present paper to

53 retrieve the lidar ratio for CALIOP-CALIPSO aerosol models.

54 The lidar ratio depends on two optical properties viz. extinction coefficient and backscattering coefficinet and

55 thus, it depends on the incident wavelength, refractive index and the size distribution of the aerosols. In real

56 atmospheric conditions, aerosols exhibit different shapes and sizes and are composed of various kinds of

57 compounds. In addition to this, various aerosol components are affected due to variations in relative humidity.

58 Thus, it is essential to study the variations in lidar ratio due to different atmospheric conditions for various

59 compositions of aerosols. Salemink et al. (1984) reported a linear increase in the lidar ratio when relative humidity

60 was increased from 40% to 80% during a field experiment details of which are not mentioned in the paper.

61 Ackermann (1998) has reported a numerical study of lidar ratio with respect to variations in relative humidity for

62 Nd:YAG wavelengths for continental, maritime and desert aerosol models where author has considered some

63 hypothetical cases for number mixing ratios of the aerosol components. He has established a non-linear

64 relationaship between relative humidity and lidar ratio. Zhao et al. (2017) used Mie theory and k-Kohler theory

65 to study the influences of aerosol hygroscopic growth on lidar ratio and used *in-situ* data collected during a field

66 campaign to establish a relationship between lidar ratio and relative humidity. Dusing et al. (2021) has also

67 established a non-linear relationship between lidar ratio and relative humidity for Central European aerosols using

68 *in-situ* data. Optical properties of aerosols are important to study the radiation balance of the Earth and climate

69 change. Optical Properties of Cloud and Aerosols (OPAC) software tool facilitates with the dataset of optical

70 properties of the aerosols and clouds and a program to extract these datasets. The standard global aerosol models

71 are considered in OPAC as given in d'Almeida et al. (1991) and Hess et al. (1998). Component mixing in aerosols

72 is based on particle number densities, which are independent of relative humidities in OPAC. However, this will

73 affect the aerosol lidar ratio.

74 Several authors have reported different lidar ratio values for different aerosol models using a variety of

75 methodologies. d'Almeida et al. (1991) have reported values of 16-22 sr for clean marine and desert models at

76 ruby wavelength when lidar ratio was estimated as ratio of extinction coefficient to phase function at 180°. They

77 have reported a value up to 80 sr for Antarctic aerosols at ruby wavelength. Anderson et al. (2000) have showed

78 a variation of 8 to 95 sr in lidar ratio values for polluted continental model at 532 nm using nephelometer data.

79 Omar et al. (2009) have reported lidar ratio values for desert, smoke, clean continental, polluted continental, clean

80 marine and polluted dust aerosols at 532 nm and 1064 nm varying between 20-70 sr using AERONET data. These

81 values are reported with 30% uncertainty and are selected as lidar ratio in CALIPSO-V1 operational algorithms.

82 The lidar ratios for polluted dust aerosols are updated to 55 sr and 48 sr at 532 nm and 1064 nm respectively, in

83 CALIPSO-V3 operational algorithm whereas lidar ratio for clean continental aerosols is updated to 53 sr at 532

84 nm in CALIPSO-V4 operational algorithm (Kim et al. 2018). Lopes et al. (2013) have reported a regional study

85 in Brazil about lidar ratio selection algorithm for CALIPSO data only at 532 nm using AERONET sun

86 photometers. They have reported the similar values for all aerosol models as used in CALIPSO-V1 algorithm by

87 Omar et al. (2009) except for polluted dust in which case the lidar ratio value is updated to 55 sr. Li et al. (2022)

88 have assessed CALIPSO-V4 lidar ratio selection algorithm by retrieving lidar ratios as combination of CALIPSO

89 columnar attenuated backscatter and Synergised Optical Depth of Aerosols (SODA) algorithms. This study has

90 ignored clean continental aerosols and has proposed elevated smoke and dusty marine aerosol models with lidar

91 ratios of 47 sr and 32 sr respectively; during night at 532 nm.

92 The present study reports a theoretical approach for estimation of lidar ratio from various sources, such as aerosol

93 models reported by Hess et al. (1998) (OPAC aerosol models), Omar et al. (2005 and 2009) for wavelengths 532

94 nm, 673 nm and 1064 nm (CALIPSO and AERONET aerosol models). The variation in lidar ratio with respect to

95 relative humidity was also studied at Nd:YAG wavelengths using OPAC (Hess et al. 1998) aerosol models. Hess

96 et al. (1998) have reported aerosol models as composition of various components contributing to different aerosol

97 types whereas Omar et al. (2005 and 2009) have reported aerosol models in terms of contribution from fine and

98 coarse particles i.e. in terms of aerosol sizes. As mentioned earlier, theoretical approach for lidar ratio estimation

99 using Mie theory is still a gap area for CALIPSO and OPAC aerosol models and thus, this study, attempts to

100 provide a physics based theoretical approach covering all types of aerosol models over the varying lidar ratio

101 values based on in-situ measurements.

102 The paper is organised into five sections. The first section presents the introductory literature review and

103 motivation behind this study. The second section outlines the data used in this study. The detailed methodology

104 and Mie theory for lidar ratio estimation is presented in the third section of this paper. The results are discussed

105 in the fourth section whereas the concluding remarks are listed in the fifth section of this paper.

2 Input Data:

107 The lidar ratio depends on aerosol size distribution, refractive index and incident wavelength. The inputs used in

108 this study are the aerosol models provided in d'Almeida et al. (1991), Ackermann (1998), Hess et al. (1998), and

109 Omar et al. (2005 and 2009).

110 Table 1 and 2 present the CALIOP-CALIPSO aerosol models and cluster classified AERONET aerosol models

111 respectively; defined in Omar et al. (2009 and 2005) at 532 nm, 673 nm and 1064nm. These data include the

112 refractive indices (in terms of real part (m_r) and imaginary part (m_i)) for each of the component aerosols along

113 with the size distribution of the aerosol in terms of median radius (r_m) and standard deviation (σ).

114   Omar et al. (2005) have reported aerosol refractive indices at 673 nm and have classified aerosols through cluster

115   analysis in six different categories numbered 1-6 viz. desert dust, biomass burning, rural, industrial pollution,

116   polluted marine and dirty pollution using AERONET data. The desert dust and polluted marine (i.e. category 1

117   and category 5) aerosol models represent the categories of aerosols originated from the natural sources whereas

118   the biomass burning, continental pollution and dirty pollution (i.e. category 2, 4, and 6) aerosol models represent

119   the aerosols emanating from the anthropogenic sources. Rural background aerosol model (i.e. category 3)

120   represent those aerosols which are observed in relatively clean atmosphere.

121   The category 1 aerosols have fine fraction by volume of 0.22 indicating that coarse particles dominate the volume

122   of this category. The mean radius and geometric standard deviation for the fine mode is of 0.12 µm and 1.48 µm

123   respectively; for this category. The refractive index of this category of aerosols is considered to be $1.45 - 0.0036i$

124   as reported in table 2. The sites considered for these category of aerosols are either desert regions, close to desert

125   regions or the sites where desert dust has been observed as a result of long-range transport. The category 2 aerosols

126   have fine fraction by volume of 0.33 whereas mean and geometric standard deviation for the fine mode is 0.14

127   µm and 1.56 µm respectively. Category 2 aerosols are dominated by coarse mode particles which have a mean

128   radius and geometric standard deviation of 3.73 µm and 2.14 µm respectively. Category 1 and category 2 aerosols

129   have single scattering albedo values of 0.94 and 0.82 respectively which are estimated using Mie theory presented

130   in this paper. These single scattering albedo values are consistent with those reported by Omar et al. (2005).

131   Category 3 aerosols are characterised by low optical depth values as they are originated from clean atmosphere.

132   These aerosols have fine fraction by volume of 0.38 indicating dominance of coarse particles. The mean radius

133   and geometric standard deviation for the fine mode is of 0.13 µm and 1.50 µm respectively. The refractive index

134   for this category of aerosols is considered to be $1.45 - 0.0092i$. The single scattering albedo value is observed to

135   0.89 for category 3 aerosols. The category 4 aerosols are found in urban centres or near urban centres and are

136   dominated by the natural pollutants such as sulfate particles (Omar et al. 2005). The refractive index for these

137   category of aerosols is considered to be $1.41 - 0.0063i$ which is representing the natural pollutants comprising

138   category 4 aerosols. The size distribution of category 4 aerosols is described by a mean radius and geometric

139   standard deviation for fine mode of 0.16 µm and 1.53 µm respectively. The mean radius and geometric standard

140   deviation for coarse mode is of 3.55 µm and 2.07 µm respectively. The single scattering albedo for these category

141   of aerosols is estimated to be 0.93.

142   The category 5 aerosols are observed at islands or at coastal regions. The fine fraction by volume is of 0.26 and

143   size distribution is described by a mean radius and geometric standard deviation for fine mode of 0.17 µm and

144   1.61 µm respectively. The refractive index for these category of aerosols is considered to be $1.39 - 0.0044i$. These

145   optical properties are resulted in the single scattering albedo of 0.94 for polluted marine aerosols. The category 6

146   aerosols are similar to category 4 aerosols with a high imaginary part of refractive index. The refractive index of

147   category 6 aerosols is considered to be $1.41 - 0.0337i$ which resulted in low single scattering albedo of 0.68. The

148   low single scattering albedo indicates that these are the aerosols with mostly carbon element in it (Omar et al.

149   2005). The size distribution of these category of aerosols is described by a mean radius and geometric standard

150   deviation of 0.14 µm and 1.54 µm respectively. The more details about these six categories of aerosols can be

151   found in Omar et al. (2005).

152   The theoretically derived lidar ratios were compared with lidar ratio derived using AERONET data for three

153   different stations classified for each of the above-mentioned six categories. The details are discussed in results

154   section of this paper.

155   Table 3, 4 and 5 collectively report the OPAC aerosol models. These aerosol models are defined in terms of their

156   size distribution with respect to relative humidity, refractive indices at 532 nm and 1064 nm and composition of

157   aerosol types in terms of number mixing ratio (μ). The lognormally distributed aerosol components were

158   considered in this study. The relative humidity was varied from 0% to 99% with intermediate steps at 50%, 70%,

159   80%, 90% and 98%. The details about OPAC aerosol models can be found in Hess et al. (1998).

160   **3   Computation of Lidar Ratio using Mie Theory:**

161   In this study, the aerosols were assumed as homogeneous isotropic spheres scattering the electromagnetic

162   radiation incident upon them. These scattering phenomenons are modelled using Mie theory, which is discussed

163   in Bohren, and Huffman (1983) and Vermote et al. (2006) and many other authors. The lidar ratio, which is defined

164   as the ratio of extinction coefficient to backscatter coefficient, is derived in the present study using the Mie theory

165   equations. The computational equations are presented here briefly, for the ready reference.

166   The Mie parameter (x) for an aerosol with refractive index, $m = n_r - in_i$ is defined as

167   $x = \frac{2\pi r}{\lambda},$ (1)

168   where r is the aerosol particle radius in micron and λ is the wavelength in micron. Here m is the refractive index

169   with real part n_r and imaginary part n_i.

170   Two complex functions $S_1(x, m, \theta)$ and $S_2(x, m, \theta)$ related to amplitude of scattered radiation that are

171   perpendicular and parallel to the plane of scattering with scattering angle θ, respectively, can be defined as

172   follows.

173   $S_1(x, m, \theta) = \sum_{n=1}^{\infty} \frac{(2n+1)}{n(n+1)} [a_n(x, m)\pi_n(cos\theta) + b_n(x, m)\tau_n(cos\theta)]$ and   (2)

174   $S_2(x, m, \theta) = \sum_{n=1}^{\infty} \frac{(2n+1)}{n(n+1)} [a_n(x, m)\tau_n(cos\theta) + b_n(x, m)\pi_n(cos\theta)],$ (3)

175   where, the complex functions $a_n(x, m)$ and $b_n(x, m)$ are given by

176   $a_n(x, m) = \frac{\Psi_n'(mx)\Psi_n(x) - m\Psi_n(mx)\Psi_n'(x)}{\Psi_n'(mx)\xi_n(x) - m\Psi_n(mx)\xi_n'(x)}$ and   (4)

177   $b_n(x, m) = \frac{m\Psi_n'(mx)\Psi_n(x) - \Psi_n(mx)\Psi_n'(x)}{m\Psi_n'(mx)\xi_n(x) - \Psi_n(mx)\xi_n'(x)},$ (5)

178   which are defined in terms of Ricatti-Bessel functions $\Psi_n(z = x \ or \ mx)$ and $\xi_n(z = x \ or \ mx)$. Ricatti-Bessel

179   functions are evaluated using their logarithmic derivatives details of which are provided in Vermote et al. (2006).

180   In order to compute the complex functions $S_1(x, m, \theta)$ and $S_2(x, m, \theta)$, the functions π_n and τ_n are computed

181   using associated Legendre polynomials. The functions π_n and τ_n are the functions of scattering angle θ. These

182   can be computed using the recurrence relations

183   $n\pi_{n+1}(cos\theta) = (2n + 1)cos\theta\pi_n(cos\theta) - (n + 1)\pi_{n-1}(cos\theta)$ and   (6)

184   $\tau_{n+1}(cos\theta) = (n + 1)cos\theta\pi_{n+1}(cos\theta) - (n + 2)\pi_n(cos\theta).$ (7)

185   which are initialised with $\pi_0(cos\theta) = 0$, $\pi_1(cos\theta) = 1$, and $\tau_0(cos\theta) = cos\theta$.

186 Using these quantities, the extinction efficiency ($Q_e(\lambda, r, m)$), dimensionless angular-scattering intensity

187 efficiency ($M_{11}(\lambda, r, m, \theta)$), the scattering efficiency ($Q_{sca}(\lambda, r, m)$), and backscattering efficiency

188 ($Q_{back}(\lambda, r, m)$) can be computed as

189
$$Q_e(\lambda, r, m) = \frac{\sigma_e(\lambda, r, m)}{\pi r^2} = \frac{2}{x^2} \sum_{n=1}^{\infty} (2n+1) \mathcal{R}e[a_n(x, m) + b_n(x, m)], \tag{8}$$

190
$$M_{11}(\lambda, r, m, \theta) = \frac{1}{2x^2}[S_1(x, m, \theta)S_1^*(x, m, \theta) + S_1(x, m, \theta)S_2^*(x, m, \theta)], \tag{9}$$

191
$$Q_{sca}(\lambda, r, m) = \frac{\sigma_{sca}(\lambda, r, m)}{\pi r^2} = \frac{2}{x^2} \sum_{n=1}^{\infty} (2n+1)[a_n(x, m)a_n^*(x, m) + b_n(x, m)b_n^*(x, m)] \text{ and} \tag{10}$$

192
$$Q_{back}(\lambda, r, m) = \frac{4}{x^2}|S_1(x, m, 180^0)|^2 = 4M_{11}(\lambda, r, m, 180^0), \tag{11}$$

193 where r is the particle radius, $\sigma_e(\lambda, r, m)$ is the extinction cross section and $\sigma_{sca}(\lambda, r, m)$ is the scattering cross

194 section.

195 Thus, the lidar ratio can be computed as

196
$$LR = \frac{Nr}{Dr} = \frac{\sum_{i=1}^{M} \int_0^\infty Q_e(\lambda, r, m_i)\pi r^2 n(r) dr}{\sum_{i=1}^{M} \int_0^\infty Q_{back}(\lambda, r, m_i)\pi r^2 n(r) dr}. \tag{12}$$

197 The single scattering albedo can be computed as

198
$$\omega_0 = \frac{\sum_{i=1}^{M} \int_0^\infty Q_{sca}(\lambda, r, m_i)\pi r^2 n(r) dr}{\sum_{i=1}^{M} \int_0^\infty Q_e(\lambda, r, m_i)\pi r^2 n(r) dr}. \tag{13}$$

199 In this study, an aerosol is considered as mixture of its constituent components. And each of the component is

200 lognormally distributed with median radius r_m and standard deviation σ. Thus,

201
$$n(r) = \frac{\mu N_{tot}}{\sqrt{2\pi} r \ln(\sigma)} exp\left[-\frac{ln^2(r/r_m)}{2ln^2\sigma}\right], \tag{14}$$

202 where μ is the number mixing ratio (i.e. normalised number particle concentration) and N_{tot} is the total number

203 density of the aerosol component.

204 The relative humidity influences the refractive index of the hygroscopic aerosol components and the effective

205 refractive index is

206
$$m_i = m_w + (m_{0,i} - m_w)\left(\frac{r_{0,i}}{r_{m,i}}\right)^3, \tag{15}$$

207 where m_w is the refractive index of the water, $m_{0,i}$ is the refractive index of the dry particle of component i and

208 $r_{0,i}$ is the median radius of the dry particle of component i.

209 The theory presented above is with the assumption of homogenous spherical isotropic aerosol particles, which

210 simplifies the computation of lidar ratio. However, if the particles are not homogenous and anisotropic then the

211 above theory may cause errors as the scattering phase function will differ to address the anisotropy. Moreover, if

212 the particles are nonhygroscopic especially when the particles are large as compared to the incident wavelength

213 then the above theory fails (Ackermann 1998).

214 ## 4   Results and Discussion:

215 ### 4.1 Lidar Ratio for AERONET and CALIPSO Aerosol Models defined in terms of particle sizes:

216 The aerosol models defined in terms of particle size by Omar et al. (2005 and 2009) were used to estimate the

217 lidar ratio for aerosol models used in operational algorithms of CALIOP-CALIPSO. Omar et al. (2005) used

218 cluster analysis for AERONET data to define the aerosol models at 673 nm. Table 6 shows the lidar ratio estimated

219 using the Mie theory for each of the six clusters defined by Omar et al. (2005). The maximum lidar ratio of 48.87

220   sr was observed for dirty pollution type of aerosols whereas the minimum of 28.76 sr was observed for desert dust

221   kind of aerosols. The lidar ratios at 532 nm are mostly discussed in literature (Ackermann 1998, Anderson et al.

222   2000, Omar et al. 2009, Lopes et al. 2013 and Kim et al. 2018 and 2022) and scanty literature is available for lidar

223   ratios at 673 nm. Moreover, these aerosol models are derived using AERONET data. Thus, the estimated lidar

224   ratios at 673 nm were compared with those of the AERONET data.

225   The data for three different stations for each of the category was selected and aerosol lidar ratio was computed

226   using equation (12) as a multiplier of 4π. Tables 7-12 show the statistics of the lidar ratio for different AERONET

227   stations belonging to different categories. The daily averages of the lidar ratios were obtained using the

228   AERONET single scattering albedo and phase function values and were compared with the Mie theory estimated

229   values. The Mie theory estimated values were observed to comply with the observed values of lidar ratios using

230   AERONET data as the theoretically estimated values were lying in between the minimum and maximum of the

231   daily lidar ratio values. The differences in the theoretical values estimated using Mie theory and those observed

232   using AERONET data were primarily due to the refractive indices of the different aerosol types present at the

233   different AERONET stations. Omar et al. (2005) had classified the different aerosol types mentioned in section 2

234   using cluster analysis and the geographical location of these AERONET stations was also considered to be an

235   important factor while classification. Thus the composition of the aerosols observed over a period of time varied

236   resulting in the variation of the refractive indices. The theoretically computed lidar ratios were based on the

237   refractive index of the centre of the cluster analysed using AERONET data before 2002 (Omar et al. 2005) whereas

238   the AERONET stations data used in this study spanned over 1998 to 2021 leading to the differences in the

239   refractive indices of the aerosol types. The shape of the aerosol particles, their size distribution and their particle

240   density present in the atmosphere may be the secondary reasons for the differences between the theoretically

241   estimated values of lidar ratio using Mie theory and the lidar ratio computed using AERONET stations data which

242   needs further investigation.

243   The aerosol models derived using the cluster analysis by Omar et al. (2005) and their respective lidar ratios were

244   used in lidar ratio selection and feature detection algorithm of CALIOP-CALIPSO (Young and Vaughan 2009).

245   These aerosol models and their respective lidar ratios used in operational algorithms of CALIOP-CALIPSO are

246   specified in Young and Vaughan (2009). These lidar ratios were subsequently updated in the V3 and V4 CALIOP-

247   CALIPSO operational algorithms (Kim et al. 2018). The basis for lidar ratio selection algorithm for CALIOP-

248   CALIPSO operational products has been the cluster analysis using the AERONET data and thus, the lidar ratios

249   were estimated using Mie theory, which gives the physical basis for the lidar ratio selection algorithm.

250   Figure 1 and 2 show the distribution of extinction and backscatter coefficients for CALIPSO aerosol models at

251   532 nm and 1064 nm; respectively. The particle sizes were varied from 0.01 μm to 5 μm and the cut-off radius

252   for fine particles was taken to be 1 μm for all CALIPSO aerosol models except clean marine aerosols in which

253   case the fine particle radius cut-off was 0.6 μm. The maxima of extinction and backscatter coefficients at 532 nm

254   and 1064 nm, for all aerosol models except clean marine aerosols was observed between 0.07 μm to 0.4 μm. In

255   case of all aerosol models, it was observed that the contribution from fine particles was more in magnitude

256   compared to that from coarser particles at 532 nm and 1064 nm except the clean marine model. In case of clean

257   marine aerosols at 1064 nm, the coarser particles were observed to contribute significantly in magnitude to the

258   extinction coefficient as compared to fine particles producing lidar ratio value of 71 sr.

259   Table 13 shows the lidar ratio values estimated for the CALIPSO aerosol models specified in Omar et al. (2009)
260   and its comparison with the lidar ratio values selected in various versions of CALIOP-CALIPSO operational
261   algorithms. It was observed that the lidar ratio values estimated using Mie theory in present study comply with
262   the lidar ratio values reported in literature for CALIPSO operational algorithms. The lidar ratio proposed for clean
263   continental model at 532 nm in CALIPSO V4 operational algorithm was 53 ± 24 sr, allowing the variation up to
264   77 sr. The Mie theory estimate for clean continental model at 532 nm was centred on 85 sr considering the
265   refractive index of the centre cluster as provided in Omar et al. (2009). The variation in refractive index will affect
266   the lidar ratio value, which was evident when compared to OPAC aerosol models where the lidar ratio of clean
267   continental aerosols was centred on 53 sr. Similar results were observed in case of clean marine aerosols at 532
268   nm and desert dust particles at 1064 nm. In case of desert dust particles at 1064 nm the variation up to 31 sr was
269   allowed in CALISPO V4 operational algorithm whereas the present study proposed lidar ratio value of 20 sr for
270   desert dust aerosols at 1064 nm. The desert dust lidar ratio at 1064 nm proposed for CALIPSO aerosol model was
271   observed to be consistent with OPAC desert aerosol model in which case lidar ratio was observed to be centred
272   on 23 sr. These results for desert aerosols at 1064 nm comply with those reported by Ackermann (1998) where
273   dry desert aerosol lidar ratio was lying just under 20 sr. The results for OPAC aerosol models are discussed in
274   detail in the subsequent section. CALISPO operational V3 algorithm allowed variation up to 68 sr in lidar ratio
275   of clean marine aerosols at 1064 nm whereas the present study estimated the value of 71 sr for clean marine
276   aerosols at 1064 nm. The theoretically estimated lidar ratio for clean marine aerosols at 532 nm was observed to
277   be consistent with that reported in the literature. The theoretically proposed value in the present study for clean
278   marine aerosols at 532 nm was 57.31 sr whereas Li et al. (2022) reported the median value of lidar ratio for clean
279   marine aerosols of 60 sr. Thus, the Mie theory estimated lidar ratio values can provide the physical basis for the
280   CALIPSO operational algorithms and can be used as look-up table to derive the vertical extinction and backscatter
281   particulate profiles using satellite data.

282   The theoretical approach proposed in this study to estimate lidar ratio for CALIPSO aerosol models was further
283   validated through estimation of single scattering albedo at 673 nm for the aerosol models classified using
284   AERONET data as described in table 2. The single scattering albedo values for AERONET aerosol models viz.
285   Category 1 to Category 6 were estimated using the above presented Mie theory as 0.94, 0.82, 0.89, 0.93, 0.94 and
286   0.68 respectively. The single scattering values at 673 nm for these AERONET aerosol models viz. Category 1 to
287   Category 6 were reported by Omar et al. (2005) as 0.93, 0.80, 0.88, 0.92, 0.93 and 0.72. The comparison between
288   the theoretically estimated and literature reported single scattering albedo values showed the percent absolute
289   difference between 1.06% to 5.56%, which validates the proposed Mie theory for estimation of lidar ratio.

290   **4.2 Lidar Ratio for OPAC Aerosol Models Defined in terms of Constituent Components:**

291   The lidar ratios were also estimated when aerosol models were specified in terms of different constituent
292   compositions as used in OPAC. The aerosol models viz. clean continental, average continental, polluted
293   continental, urban, clean maritime, maritime tropical, polluted maritime, desert, arctic and antarctic were used in
294   the present study to estimate the lidar ratio using Mie theory. The number mixing ratios as specified in OPAC
295   software by Hess et al. (1998) were used in the present study to define the size distribution of aerosols. The relative
296   humidity causes an increase in size of a hygroscopic particle such as water soluble, sea salt and sulfate particles.
297   Thus, the backscattering and extinction profiles of these particles are significantly affected.

298 Figure 3 shows the variation in backscatter coefficient of the continental and maritime aerosols at 532 nm and

299 1064 nm. The backscattering coefficient of continental and maritime aerosols were observed to increase when

300 relative humidity was increased from 0% to 99%. The increase in backscattering with relative humidity was

301 considerably higher in polluted continental, urban and polluted maritime aerosols as compared to clean continental

302 and clean maritime aerosols at 532 nm and 1064 nm. Clean maritime and tropical maritime aerosols were observed

303 to have equivalent backscattering coefficients due to their equivalent composition of water soluble and sea salt

304 particles.

305 Figure 4 shows the variation in backscattering coefficients of the desert, arctic and antarctic aerosol models at 532

306 nm and 1064 nm. The Antarctic aerosols showed a sharp and significant increase in their backscattering

307 coefficients at 532 nm and 1064 nm. The increase in backscattering coefficients was observed to be more at 1064

308 nm compared to 532 nm. This causes the decrease in lidar ratio at 1064 nm as compared to that at 532 nm as can

309 be observed from figure 6. Increase in backscattering coefficient with relative humidity at 532 nm and 1064 nm

310 will cause increase or decrease in lidar ratio with respect to relative humidity depending upon the rate at which

311 the extinction and backscattering coefficients are increasing or decreasing.

312 The variation in lidar ratios of continental and maritime aerosol models with reference to relative humidity at 532

313 nm and 1064 nm is as shown in figure 5. The lidar ratio showed an increase in values for polluted continental and

314 polluted maritime aerosols over the clean continental and clean maritime aerosols. This increase was mainly

315 observed due to greater contribution of soot particles in the polluted aerosols. An increase in lidar ratio values was

316 observed at 532 nm and 1064 nm when relative humidity was increased from 80% to 99% in all types of

317 continental and maritime aerosols. The decrease in lidar ratio when relative humidity was increased from 0% to

318 80% was observed due to decrease in lidar ratio of the water soluble particles which are hygroscopic in nature.

319 This decrease was primarily due to significant decrease in the imaginary part of the refractive index of water

320 soluble component due to relative humidity. Continental and Maritime aerosols are dominated by water soluble

321 particles as defined in OPAC and thus an initial decrease and a gradual increase in lidar ratio values was observed

322 at 532 nm and 1064 nm when relative humidity was increased from 0% to 99%.

323 The lidar ratio values of the clean continental model and clean maritime aerosol models at 532 nm and 1064 nm

324 where observed to be centred around 53 sr to 51 sr with varying relative humidity. This is mainly because of the

325 composition of aerosol models as defined in OPAC. In both, clean continental and clean maritime models, water

326 soluble particles were dominant which are smaller in size as compared to the sea salt particles. However, in OPAC

327 the number mixing ratio of sea salt particles which are coarser particles, is very low as compared to finer water

328 soluble particles; which is not the case in CALIPSO clean marine aerosol model. In CALIPSO clean marine

329 model, though coarser particles are more in proportion their contribution to the backscattering and extinction

330 coefficient was observed to be less in magnitude as compared to the fine particles at 532 nm. Thus, the resulting

331 lidar ratio values for CALIPSO aerosol model were centred on 57 sr at 532 nm, which was consistent with the

332 results for OPAC clean maritime aerosol model.

333 The urban aerosols showed a significant increase in the lidar ratio values at 532 nm and 1064 nm compared to

334 other continental aerosols. The dry urban aerosols showed a lidar ratio of 74.88 sr and 61.73 sr at 532 nm and

335 1064 nm respectively; whereas dry clean continental aerosols exhibited the lidar ratio of 53.59 sr and 23.9 sr at

336 532 nm and 1064 nm respectively. This significant increase in lidar ratio values of urban aerosols is primarily due

337 to scattering soot particles. Insoluble particles hardly have any impact on lidar ratio values of urban and continental

338 aerosols due to their very small composition. Similar results were observed when polluted maritime particles were

339 compared to the clean maritime particles.

340 The variation in lidar ratios of desert, arctic and antarctic aerosols with respect to relative humidity is as shown in

341 figure 6. The lidar ratio values at 532 nm were observed to be greater than those at 1064 nm values for desert and

342 antarctic aerosols. The dry desert dust lidar ratio at 532 nm was observed to be 55.32 sr. This result comply with

343 the values for desert dust lidar ratio at 532 nm reported in literature by Muller et al. (2007), Omar et al. (2009),

344 Kim et al. (2018) and Li et al. (2022). The lidar ratio values showed a decrease with relative humidity except the

345 lidar ratio values of antarctic aerosols at 532 nm and 1064 nm. The model of arctic aerosols that is used in the

346 present study is for spring season when the arctic aerosols are mainly the soot particles. Thus, a decrease in lidar

347 ratio values with relative humidity was observed in arctic aerosols as it was in polluted continental and urban

348 aerosols at 1064 nm.

349 The lidar ratio of dry Antarctic aerosols was observed to be 57.73 sr at 532 nm and 20.90 sr at 1064 nm. The

350 summertime model of Antarctic aerosols as defined in OPAC was used in the present study where the Antarctic

351 aerosols are dominated by the sulfate particles. Sulfate particles are hygroscopic in nature with significant large

352 sizes as compared to water soluble particles. The imaginary part of refractive index of sulfate particles in

353 considerably small as compared to water soluble particles at 532 nm and 1064 nm. Thus, a sharp increase in lidar

354 ratio of sulfate particles was observed when relative humidity was increased from 0% to 99% as opposed to

355 continental, maritime and desert aerosol models.

356 **5   Conclusions:**

357 This paper presented a complex theoretical approach for estimating lidar ratio through Mie theory using CALIPSO

358 and OPAC aerosol models. The lidar ratios were estimated at three wavelengths viz. 532 nm, 673 nm and 1064

359 nm. Mie theory estimated lidar ratios at 673 nm were compared with AERONET data-derived lidar ratios at 675

360 nm and Mie theory estimated lidar ratios at 673 nm were observed to lie between the minima and maxima of the

361 AERONET data-derived lidar ratios at 675 nm. Mie theory estimated lidar ratio values for CALIPSO aerosol

362 models were in good agreement with those reported in literature for CALIPSO operational algorithm. Thus,

363 theoretically estimated lidar ratios for CALIPSO aerosol models may be used in future for CALIPSO operational

364 algorithms. CALIPSO aerosol models were specified in terms of number mixing ratio of the fine and coarse

365 particles instead of component particle type and fine particles were observed to have more significant contribution

366 towards extinction and backscattering coefficient despite their low mixing ratio as compared to coarse particles.

367 Thus, Mie theory derived lidar ratio values provide the physical basis for the lidar ratio selection algorithm for

368 derivation of vertical extinction and backscatter particulate profiles using CALIPSO data.

369 The dependence of lidar ratio with relative humidity was analysed using OPAC aerosol models including Arctic

370 and Antarctic aerosols where each aerosol type was identified with the corresponding number mixing ratio of the

371 component particles. The lidar ratio was observed to decrease when relative humidity was increased from 0% to

372 80% and a gradual increase in lidar ratio was observed when relative humidity was increased further to 99%. This

373 phenomenon is the result of dominance of hygroscopic water-soluble particles constituting clean continental, clean

374 marine, tropical continental and desert aerosols. The increase in number mixing ratio of soot particles showed an

375 overall increase in the lidar ratio values of polluted continental, urban and polluted marine aerosols over clean

376 continental and clean marine particles. The soot particles dominate the urban aerosols and arctic aerosols, which
377 are non-hygroscopic fine particles. Thus, a decrease in lidar ratio of urban and arctic aerosols was observed with
378 respect to relative humidity and an increase in the backscattering coefficient of urban and arctic aerosols was
379 observed with relative humidity due to contribution from the hygroscopic water-soluble particles that grows in
380 size in presence of water vapour in the atmosphere. In case of Antarctic aerosols, the lidar ratio was observed to
381 increase with respect to relative humidity due to hygroscopic sulfate particles that backscattered heavily in
382 presence of water vapour.

383 The method presented in this study to estimate the lidar ratio using Mie theory is valid only for spherical, isotropic,
384 non-hygroscopic particles and thus there can be possible errors occurring in the lidar ratio values especially when
385 the aerosols are anisotropic and hygroscopic in nature. Thus, there is future scope for the present study to extend
386 it to theoretical estimation of lidar ratio in case of hygroscopic and anisotropic non-homogeneous particles.

6 Acknowledgement:

388 The authors are thankful to Shri. N. M. Desai, Director-SAC (ISRO), Dr. Rashmi Sharma, DD-EPSA/SAC and
389 Dr. B. K. Bhattacharya, GD-AESG/EPSA/SAC for their support and encouragement to carry out this work. The
390 authors are thankful to all those who directly and indirectly supported in realisation of this activity. This research
391 is carried out under SAC, ISRO's TDP/R&D program.

7 Competing Interests:

393 This is being declared that none of the authors have any competing interests.

8 References:

395 Ackermann, J.: The Extinction-to-Backscatter Ratio of Tropospheric Aerosol: A Numerical Study, J. Atm. Ocea.
396 Tech., 15, 1043-1050, 1998.
397 Anderson, T. L., Masonis, S. J., Covert, D. S., Charlson, R. J., and Rood, M. J.: In situ measurement of the Aerosol
398 Extinction-to-Backscatter Ratio at a Polluted Continental Site, JGR, 105, 26907-26915, 2000.
399 Ansmann, A., Wagner, F., Müller, D., Althausen, D., Herber, A., von Hoyningen-Huene, W., and Wandinger, U.:
400 European Pollution Outbreaks during ACE 2: Optical Particle Properties Inferred from Multiwavelength Lidar
401 and Star-Sun Photometry, J. Geophys. Res.-Atmos., 107, 8–14, 2002.
402 Bohren, C. F., and Huffman, D. R.: Absorption and Scattering of Light by Small Particles, Wiley and Sons, 530
403 pp., 1983.
404 d'Almeida, G., Koepke, P., and Shettle, E. P.: Atmospheric Aerosols: Global Climatology and Radiative
405 Characteristics, A. Deepak, 561 pp., 1991
406 Dusing, S., Ansmann A., Baars, H., Corbin, J. C., Denjean, C., Gysel-Beer, M., Muller, T., Poulain, L., Siebert,
407 H., Spindler, G., Tuch, T., Wehner, B., and Wiedensohler, B.: Measurement Report: Comparison of Airborne, in-
408 situ Measured, Lidar-based and Modeled Aerosol Optical Properties in the Central European Background –
409 Identifying Sources of Deviations, Atmos. Chem. Phys., 21, 16745-16773, 2021.

410   Hess, M., Koepke, P., and Schult, I.: Optical Properties of Aerosols and Clouds: The Software Package OPAC,

411   Bull. Amer. Meteor. Soc., 79, 831-844, 1998.

412   Kim, M. H., Omar, A. H., Tackett, J. L., Vaughan, M. A., Winker, D. M., Trepte, C. R., Hu, Y., Liu, Z., Poole, L.

413   R., Pitts, M. C., Ka, J., Magill, E.: The CALIPSO version 4 Automated Aerosol Classification and Lidar Ratio

414   Selection Algorithm, Atm. Meas. Tech., 11, 6107-6135, 2018.

415   Li, Z., Painemal, D., Schuster, G., Clayton, M., Ferrare, R. A., Vaughan, M. A., Josset, D., Kar, J., Trepte, C. R.:

416   Assessment of Tropospheric CALIPSO Version 4.2 Aerosol Types over the Ocean using Independent CALIPSO-

417   SODA Lidar Ratios, Atm. Meas. Tech., 15, 2745-2766, 2022.

418   Lopes, F. J. S., Landulfo, E., and Vaughan, M. A.: Evaluating CALIPSO's 532 nm lidar ratio selection algorithm

419   using AERONET sun photometers in Brazil, Atmos. Meas. Tech., 6, 3281-3299, 2013.

420   Muller, D., Ansmann, A., Mattis, I., Tesche, M., Wandinger, U., Althausen, D., and Pisani, G. : Aerosol-type-

421   dependent Lidar Ratios Observed with Raman Lidar, JGR, 112, D16202, 2007.

422   Omar, A. H., Won, J. G., Winker, D. M., Yoon, S. C., Dubovik, O., and McCormick, M. P.: Development of

423   Global Aerosol Models using Cluster Analysis of Aerosol Robotic Network (AERONET) Measurements, JGR,

424   110, 1-14, 2005.

425   Omar, A. H., Winker, D. M., Kittaka, C., Vaughan, M. A., Liu, Z., Hu, Y., Trepte, C. R., Rogers, R. R., Ferrare,

426   R. A., Lee, K. P., Kuehn, R. E., and Hostetler, C. A.: The CALIPSO Automated Aerosol Classification and Lidar

427   Ratio Selection Algorithm, J. Atm. Ocea. Tech., 26, 1994-2014, 2009.

428   Salemink, H., Schotanus, P., and Bergwerff, J. B.: Quantitative Lidar at 532 nm for Vertical Extinction Profiles

429   in the Lidar Solution, Appl. Phys., 34B, 187–189, 1984.

430   Takamura, T., Sasano Y., and Hayasaka T.: Tropospheric Aerosol Optical Properties Derived from Lidar, Sun

431   Photometer, and Optical Particle Counter Measurements, Appl. Opt., 33, 7132–7140, 1994.

432   Vermote, E. F., Tanre, D., Deuze, J. L., Herman, M., Morcrette, J. J., Kotchenova, S. Y.: Second Simulation of a

433   Satellite Signal in the Solar Spectrum – Vector (6SV) User Guide Version 3 – Part II, available at

434   (http://6s.ltdri.org/), 2006.

435   Young, S. A. and Vaughan, M. A.: The Retrieval of Profiles of Particulate Extinction from Cloud-Aerosol Lidar

436   Infrared Pathfinder Satellite Observations (CALIPSO) data: Algorithm Description, J. Atm. Ocea. Tech., 26,

437   1105-1119, 2009.

438   Zhao, G., Zhao, C., Kuang, Y., Tao, J., Tan, W., Bian, W., Li, J. and Li, C.: Impact of Aerosol Hygroscopic

439   Growth on Retrieving Aerosol Extinction Coefficient Profiles from Elastic-Backscatter Lidar Signals, Atmos.

440   Chem. Phys., 17, 12133-12143, 2017.

441

442

443

444

445
446   **Figure 1:** Extinction and Backscatter Distribution at 532 nm of CALIPSO Aerosol Models viz. (a) Dust (b)
447   Smoke (c) Clean Continental (d) Polluted Continental (e) Clean Marine and (f) Polluted Dust
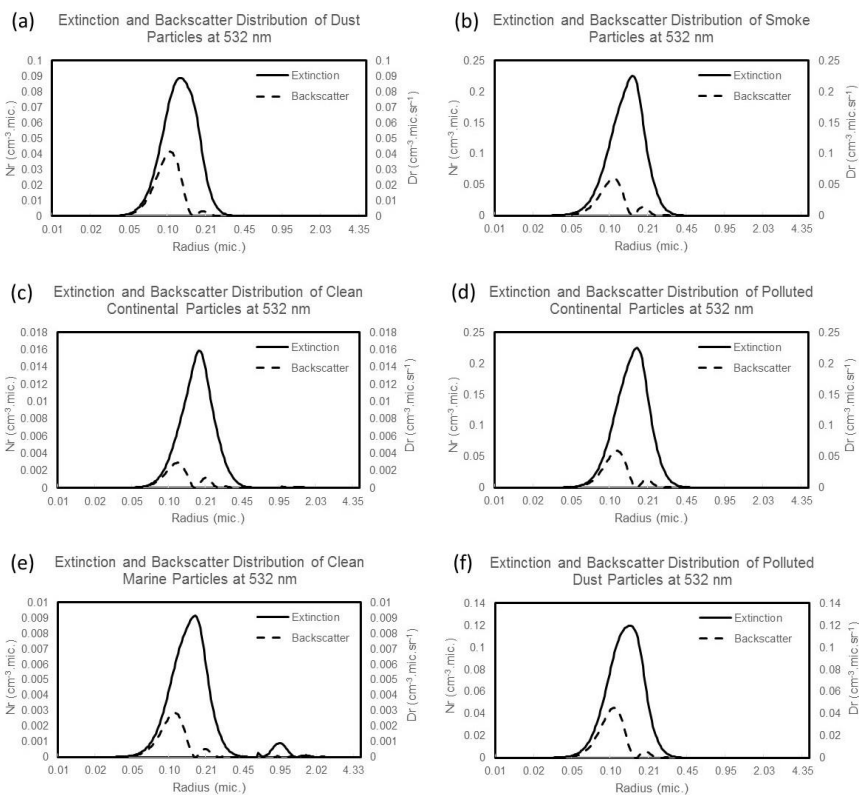
448

449

450

451

452

453

454

455
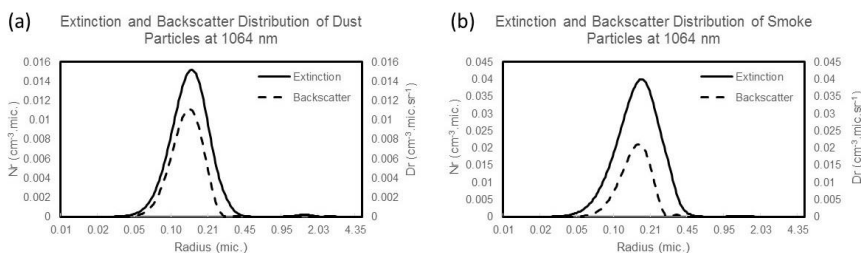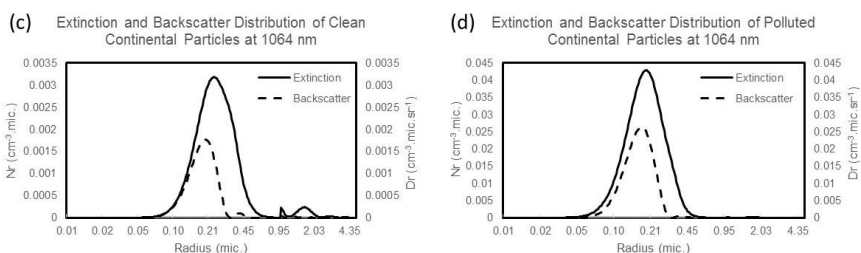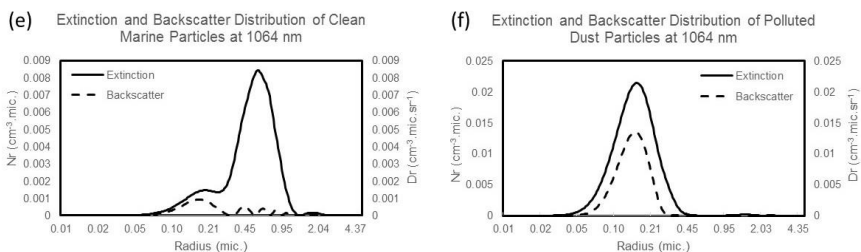
456
457
458
459 **Figure 2:** Extinction and Backscatter Distribution at 1064 nm of CALIPSO Aerosol Models viz. (a) Dust (b)
460 Smoke (c) Clean Continental (d) Polluted Continental (e) Clean Marine and (f) Polluted Dust
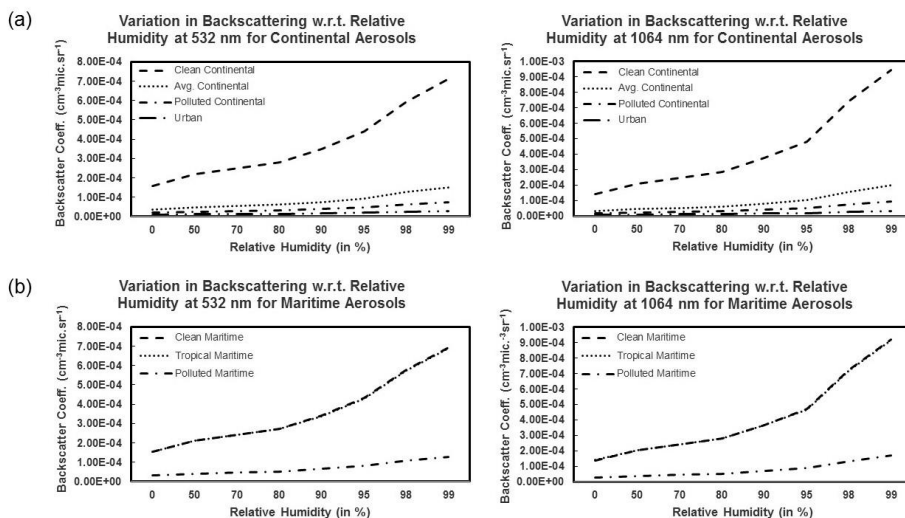
461
462 **Figure 3:** Variation in Backscattering Coefficient w.r.t. Relative Humidity for (a) Continental Aerosols and (b)
463 Maritime Aerosols at 532 nm and 1064 nm.

464

465
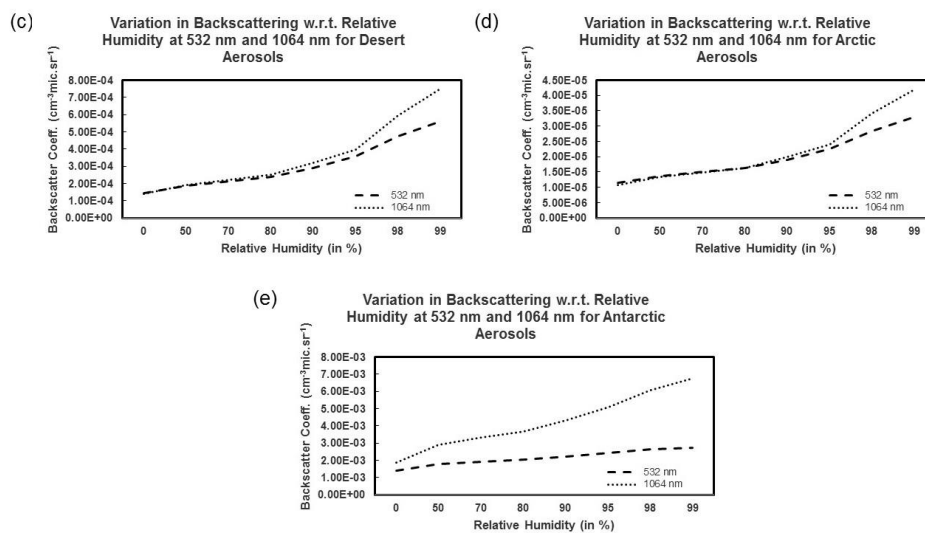
Figure 4: Variation in Backscattering Coefficient w.r.t. Relative Humidity for (c) Desert Aerosols and (d) Arctic Aerosols and (e) Antarctic Aerosols at 532 nm and 1064 nm.

468

469
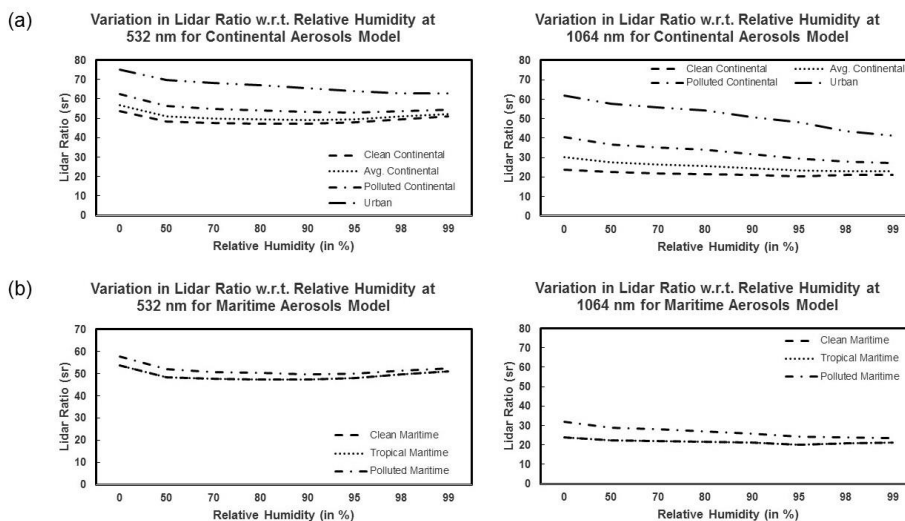
Figure 5: Variation in Lidar Ratio w.r.t. Relative Humidity for (a) Continental Aerosols and (b) Maritime Aerosols at 532 nm and 1064 nm.
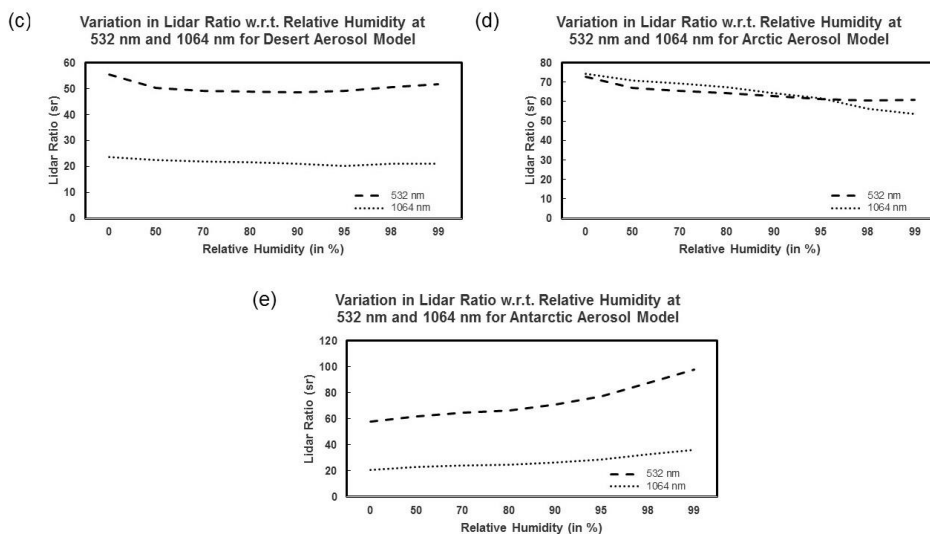
472
473 **Figure 6**: Variation in Lidar Ratio w.r.t. Relative Humidity for (c) Desert Aerosols and (d) Arctic Aerosols and
474 (e) Antarctic Aerosols at 532 nm and 1064 nm.

475

476

477

478

479

480

481

482

483

484

485

486

487

488

489

490

491

492

493   **Table 1**: Physical and Optical Properties of CALIPSO Aerosol Models (Omar et al. 2009)

Aerosol	$m_{r,532}$	$m_{i,532}$	$m_{r,1064}$	$m_{i,1064}$	$r_{m,fine}$	σ_{fine}	$r_{m,coarse}$	σ_{coarse}	μ_{fine}
Dust	1.414	0.0036	1.495	0.0043	0.1165	1.4813	2.8329	1.9078	0.223
Smoke	1.517	0.0234	1.541	0.0298	0.1436	1.5624	3.7260	2.1426	0.329
Clean Continental	1.380	0.0001	1.380	0.0001	0.20556	1.6100	2.6334	1.8987	0.050
Polluted Continental	1.404	0.0063	1.439	0.0073	0.1577	1.5257	3.5470	2.0650	0.531
Clean Marine	1.400	0.0050	1.400	0.0050	0.1500	1.6000	1.2160	1.6000	0.025
Polluted Dust	1.452	0.0109	1.512	0.0137	0.1265	1.5112	3.1617	1.9942	0.241

494

495   **Table 2**: Physical and Optical Properties of AERONET Aerosol Models at 673 nm classified using Cluster
496   Analysis (Omar et al. 2005)

Aerosol	$m_{r,673}$	$m_{i,673}$	$r_{m,fine}$	σ_{fine}	$r_{m,coarse}$	σ_{coarse}	μ_{fine}
Category 1	1.4520	0.0036	0.117	1.482	2.834	1.908	0.22
Category 2	1.5202	0.0245	0.144	1.562	3.733	2.144	0.33
Category 3	1.4494	0.0092	0.133	1.502	3.590	2.104	0.38
Category 4	1.4098	0.0063	0.158	1.526	3.547	2.065	0.53
Category 5	1.3943	0.0044	0.165	1.611	3.268	1.995	0.26
Category 6	1.4104	0.0337	0.140	1.540	3.556	2.134	0.49

497

498   **Table 3**: Size Distribution of Aerosol Components for Models used in OPAC for Different Relative Humidities
499   (d'Almeida et al. 1991 and Ackermann 1998)

Component	r_m (0%)	r_m (50%)	r_m (70%)	r_m (80%)	r_m (90%)	r_m (95%)	r_m (98%)	r_m (99%)	σ
Water Soluble	0.0212	0.0262	0.0285	0.0306	0.0348	0.0399	0.0476	0.0534	2.239
Insoluble	0.4710	0.4710	0.4710	0.4710	0.4710	0.4710	0.4710	0.4710	2.512
Soot	0.0118	0.0118	0.0118	0.0118	0.0118	0.0118	0.0118	0.0118	2.000
Mineral (nuc.)	0.0700	0.0700	0.0700	0.0700	0.0700	0.0700	0.0700	0.0700	1.950
Mineral (acc.)	0.3900	0.3900	0.3900	0.3900	0.3900	0.3900	0.3900	0.3900	2.000
Mineral (coa.)	1.9000	1.9000	1.9000	1.9000	1.9000	1.9000	1.9000	1.9000	2.150
Mineral (trans.)	0.5000	0.5000	0.5000	0.5000	0.5000	0.5000	0.5000	0.5000	2.200
Sea Salt (acc.)	0.2090	0.3360	0.3780	0.4160	0.4970	0.6050	0.8010	0.9950	2.030
Sea Salt (coa.)	1.7500	2.8200	3.1700	3.4900	4.1800	5.1100	6.8400	8.5900	2.030
Sulfate	0.0695	0.0983	0.1090	0.1180	0.1350	0.1580	0.1950	0.2310	2.030

500

501

502 **Table 4**: Refractive Indices of the Aerosol Components for the OPAC Aerosol Models used in this study
503 (d'Almeida et al. 1991 and Ackermann 1998)

Component	$m_{r,532}$	$m_{i,532}$	$m_{r,1064}$	$m_{i,1064}$
Water Soluble	1.530	5.64×10^{-3}	1.520	1.64×10^{-2}
Insoluble	1.530	8.0×10^{-3}	1.510	8.00×10^{-3}
Soot	1.750	4.46×10^{-1}	1.760	4.43×10^{-1}
Mineral	1.530	6.33×10^{-3}	1.530	4.30×10^{-3}
Sea Salt	1.500	1.12×10^{-8}	1.470	1.95×10^{-4}
Sulfate	1.430	1.00×10^{-8}	1.423	1.50×10^{-6}
Water	1.333	1.61×10^{-9}	1.326	1.39×10^{-5}

504

505 **Table 5**: Composition of Aerosol Models used in OPAC (Hess et al. 1998)

Aerosol Types	Components	Number Mixing Ratio μ_i
Clean Continental	Water soluble	1.000
	Insoluble	0.577×10^{-4}
Average Continental	Water Soluble	0.458
	Insoluble	0.261×10^{-4}
	Soot	0.542
Polluted Continental	Water Soluble	0.314
	Insoluble	0.120×10^{-4}
	Soot	0.686
Urban	Water Soluble	0.177
	Insoluble	0.949×10^{-5}
	Soot	0.823
Clean Maritime	Water Soluble	0.987
	Sea Salt (acc.)	0.132×10^{-1}
	Sea Salt (coa.)	0.211×10^{-5}
Tropical Maritime	Water Soluble	0.983
	Sea Salt (acc.)	0.167×10^{-1}
	Sea Salt (coa.)	0.217×10^{-5}
Polluted Maritime	Water Soluble	0.422
	Sea Salt (acc.)	0.222×10^{-2}
	Sea Salt (coa.)	0.356×10^{-6}
	Soot	0.576
Desert	Water Soluble	0.870
	Mineral (nuc.)	0.117
	Mineral (acc.)	0.133×10^{-1}
	Mineral (coa.)	0.617×10^{-4}
Arctic	Water Soluble	0.197
	Insoluble	0.152×10^{-5}
	Sea Salt (acc.)	0.288×10^{-3}
	Soot	0.803
Antarctic	Sulfate	0.998
	Sea Salt (acc.)	0.109×10^{-2}
	Mineral (trans.)	0.123×10^{-3}

506

507

508

Table 6: Lidar Ratio (in sr) estimated using Mie theory for Omar et al. (2005) Aerosol Models

Aerosol Model	Desert Dust (Category-1)	Biomass Burning (Category -2)	Rural (Background) (Category-3)	Industrial Pollution (Category-4)	Polluted Marine (Category-5)	Dirty Pollution (Category- 6)
673 nm	28.68	46.92	36.27	44.20	45.18	48.87

510

Table 7: Lidar Ratio (in sr) Comparison between Theoretical values estimated using Mie Theory and In-situ values using Category-1 AERONET Data

Site/Year	2017	2018	2019	2020	2021	Mie Theory Estimate
Kanpur	53.67	47.32	50.31	54.12	50.46	28.68
Min.	36.06	21.31	30.76	32.03	29.41	
Max.	92.52	78.92	86.23	83.53	79.75	
	1998	**1999**	**2004**	**2005**	**2006**	
Bahrain	47.82	37.00	40.79	37.66	34.88	28.68
Min.	37.40	28.32	31.43	27.78	27.68	
Max.	69.67	81.69	53.60	64.40	45.83	
	2017	**2018**	**2019**	**2020**	**2021**	
Banizoumbou	49.96	52.04	50.98	49.88	51.12	28.68
Min.	27.80	29.08	37.20	32.10	41.83	
Max.	65.81	67.73	70.83	70.75	72.14	

513

Table 8: Lidar Ratio (in sr) Comparison between Theoretical values estimated using Mie Theory and In-situ values using Category-2 AERONET Data

Site/Year	2001	2002	2003	2004	2005	Mie Theory Estimate
Abracos Hill	52.95	53.89	51.87	50.52	55.30	46.92
Min.	44.99	41.63	32.30	44.24	39.87	
Max.	60.44	66.43	63.01	57.72	65.54	
	2016**	**2017**	**2018**	**2019**	**2020***	
Skukuza	38.47	49.37	43.01	44.04	63.24	46.92
Min.	19.14	32.50	34.98	28.56	63.24	
Max.	49.70	101.24	52.74	68.14	63.24	
	2014	**2015**	**2016**	**2017**	**2018**	
IMS Metu Erdemli	54.47	42.50	51.24	58.80	49.26	46.92
Min.	22.54	27.64	31.90	35.90	27.83	
Max.	69.72	61.70	73.60	75.06	67.43	

516 *Only single data value is available
517 **The data has an outlier. Without outlier the value of LR is 43.30 sr.

518

519

520

521

522 **Table 9**: Lidar Ratio (in sr) Comparison between Theoretical values estimated using Mie Theory and In-situ
523 values using Category-3 AERONET Data

Site/Year	2002	2003	2005	2006	2009*	Mie Theory Estimate
Konza EDC	52.25	43.95	54.47	39.38	47.83	36.27
Min.	39.64	32.40	37.32	38.32	35.30	
Max.	64.46	73.75	85.26	40.45	58.52	
	2012	**2017**	**2018**	**2020**	**2021****	
Sevilleta	44.47	48.17	42.10	58.52	53.53	36.27
Min.	34.65	37.09	31.75	33.45	27.39	
Max.	56.64	57.99	56.59	78.83	72.29	
	2015	**2017**	**2018**	**2020**	**2021**	
Rimrock	46.45	49.98	47.41	47.43	47.65	36.27
Min.	37.53	35.03	29.97	39.36	33.47	
Max.	52.55	60.36	57.35	58.93	63.86	

524 *Only two data values are available
525 **The data has an outlier. Without outlier the value of LR is 50.40 sr.

526 **Table 10**: Lidar Ratio (in sr) Comparison between Theoretical values estimated using Mie Theory and In-situ
527 values using Category-4 AERONET Data

Site/Year	2009	2012	2013	2014	2015	Mie Theory Estimate
Mexico City	54.44	56.86	56.99	64.40	63.40	44.20
Min.	23.16	37.61	39.66	47.48	36.68	
Max.	87.92	77.17	91.83	81.93	99.16	
	2003	**2004**	**2005**	**2006**	**2007**	
Moscow MSU MO	55.28	57.45	53.84	43.03	49.61	44.20
Min.	46.25	43.76	37.77	30.15	33.79	
Max.	68.83	71.03	77.44	55.44	68.28	
	2015	**2016**	**2017**	**2018**	**2019**	
GSFC	59.15	55.56	53.15	58.07	52.68	44.20
Min.	39.82	47.01	50.18	40.18	40.04	
Max.	67.93	60.78	55.15	68.84	61.79	

528 **Table 11**: Lidar Ratio (in sr) Comparison between Theoretical values estimated using Mie Theory and In-situ
529 values using Category-5 AERONET Data

Site/Year	2002	2003	2011*	2012	2013	Mie Theory Estimate
Arica	62.45	69.22	67.68	73.63	62.94	45.18
Min.	44.66	52.14	67.68	69.62	41.86	
Max.	90.27	86.74	67.68	76.62	77.02	
	2004	**2005**	**2007**	**2008**	**2009**	
La Parguera	47.91	51.00	45.00	47.64	46.38	45.18
Min.	45.70	48.91	37.10	45.12	39.01	
Max.	50.72	56.92	51.73	50.99	52.49	
	2013	**2014**	**2015**	**2016**	**2017**	
Ascension Island	54.55	55.31	59.29	52.54	70.73	45.18
Min.	43.57	50.08	36.15	41.35	48.15	
Max.	67.64	62.07	74.13	67.57	92.67	

530 *Only single data value is available

531 **Table 12**: Lidar Ratio (in sr) Comparison between Theoretical values estimated using Mie Theory and In-situ
532 values using Category-6 AERONET Data

Site/Year	2017	2018	2019	2020*	2021	Mie Theory Estimate
Dalanzadgad	52.80	41.68	47.58	37.85	47.43	48.87
Min.	39.46	32.05	41.55	37.85	38.27	
Max.	66.15	51.32	50.77	37.85	56.60	
	2016**	**2017**	**2018**	**2019**	**2020***	
Skukuza	38.47	49.37	43.01	44.04	63.24	48.87
Min.	19.14	32.50	34.98	28.56	63.24	
Max.	49.70	101.24	52.74	68.14	63.24	
	2014	**2015**	**2016**	**2017**	**2018**	
IMS Metu Erdemli	54.47	42.50	51.24	58.80	49.26	48.87
Min.	22.54	27.64	31.90	35.90	27.83	
Max.	69.72	61.70	73.60	75.06	67.43	

533 *Only single data value is available
534 **The data has an outlier. Without outlier the value of LR is 43.30 sr.

536 **Table 13**: Lidar Ratio (in sr) for Aerosol Models in CALIPSO Operational Algorithm

Wavelength/ Aerosol Model	Dust	Smoke (Biomass Burning)	Clean Continental	Polluted Continental	Clean Marine	Polluted Dust
Omar et al. (2009) CALIPSO V1 (based on in-situ measurements)						
532 nm	40	70	35	70	20	65
1064 nm	55	40	30	40	45	30
Lopes et al. (2013) CALIPSO LR Selection Algo. Evaluation (Mean ± S.D.)						
532 nm	40 ± 20	70 ± 28	35 ± 16	70 ± 25	20 ± 6	55 ± 22
Kim et al. (2018) CALIPSO V3 Operational Algo. (based on in-situ measurements)						
532 nm	40 ± 20	70 ± 25	35 ± 16	70 ± 25	20 ± 6	55 ± 22
1064 nm	55 ± 17	30 ± 14	30 ± 17	30 ± 14	45 ± 23	48 ± 24
Kim et al. (2018) CALIPSO V4 Operational Algo. (based on in-situ measurements)						
532 nm	44 ± 9	70 ± 25	53 ± 24	70 ± 25	23 ± 5	55 ± 22
1064 nm	44 ± 13	30 ± 14	30 ± 17	30 ± 14	23 ± 5	48 ± 24
Li et al. (2022) CALIPSO LR Selection Algo. Evaluation using SODA (Mean ± S.D.)						
532 nm (D)	42 ± 19	45 ± 17	-	45 ± 17	33 ± 15	52 ± 19
532 nm (N)	37 ± 13	57 ± 18	-	57 ± 18	33 ± 16	51 ± 18
In-house Derived in this study using Mie Theory						
532 nm	38.72	63.37	85.98	64.73	57.31	48.22
1064 nm	20.11	33.68	31.98	26.44	71.11	25.56